PCCP

PAPER

View Article Online
View Journal | View Issue

Cite this: *Phys. Chem. Chem. Phys.*, 2015, **17**, 13559

A density functional theory insight towards the rational design of ionic liquids for SO_2 capture†

Gregorio García,[a] Mert Atilhan[b] and Santiago Aparicio*[a]

Received 6th January 2015,
Accepted 16th April 2015

DOI: 10.1039/c5cp00076a

www.rsc.org/pccp

A systematic density functional theory (DFT) analysis has been carried out to obtain information at the molecular level on the key parameters related to efficient SO_2 capture by ionic liquids (ILs). A set of 55 ILs, for which high gas solubility is expected, has been selected. SO_2 solubility of ILs was firstly predicted based on the COSMO-RS (Conductor-like Screening Model for Real Solvents) method, which provides a good prediction of gas solubility data in ILs without prior experimental knowledge of the compounds' features. Then, interactions between SO_2 and ILs were deeply analyzed through DFT simulations. This work provides valuable information about required factors at the molecular level to provide high SO_2 solubility in ILs, which is crucial for further implementation of these materials in the future. In our opinion, systematic research on ILs for SO_2 capture increases our knowledge about those factors which could be controlled at the molecular level, providing an approach for the rational design of task-specific ILs.

1. Introduction

Air pollution is attracting increasing attention throughout the world. Among the main air pollutants, sulfur dioxide (SO_2), which is mainly emitted through the combustion of fossil based fuels, is causing serious harm to the environment and human health.[1,2] At the same time, SO_2 is a useful source of many intermediates in chemical synthesis.[3] As a matter of fact, there is general interest in the design and improvement of methods for SO_2 capture. Although several methods have been developed for this purpose, all of them have several drawbacks. For instance, an effective method based on flue gas desulfurization (FGD) needs a large amount of water and subsequent treatment of the consequent waste, in order to prevent excessive amounts of calcium sulphate that lead to secondary pollution in the environment. Other methods, such as amine scrubbing, are affected by solvent loss and degradation due to the low volatility and stability of amine solutions.[2,4,5]

In recent years, ionic liquids (ILs) have demonstrated their effectiveness for acid-gas removal from flue gas such as SO_2[2,3,5–9] and CO_2.[8–14] In addition, ILs contain unique properties, including good thermal and chemical stability, non-flammability and most distinctly they have almost null vapor pressure. All these features have been proved to be useful in chemical processes to replace volatile organic compounds. Nonetheless, the major advantage of ILs is the possibility to design task-specific solvents through the adequate cation–anion combinations, which requires a deep understanding of the structure–property relationship.[9,15] There is a large collection of compounds (approximately about $\sim 10^6$ when considering only "pure" ILs), and thus, system approaches on the ability of ILs for acid gas capture are useful in the selection of ILs for SO_2 storage. Unfortunately, the larger number of ILs hinders systematic experimental studies on a huge number of ILs, due to the economical and temporal cost as well as limited experimental resources. Having mentioned the cost of experimental difficulties and cost hurdles associated with broad screening of ILs for acid-gas removal, density functional theory (DFT) simulations have proven their ability to provide valuable indications and guide to the experimentalists. As a matter of fact, DFT is a suitable tool for the analysis of the interactions between ILs and gas molecules at the nanoscopic level, which allow a deeper knowledge of the structure–property relationship. Most of the reported DFT studies only consider CO_2.[7,12,13,16,17] Though, some researches leading with SO_2 capture have been reported.[7,17]

There are few recent studies that address utilization of ILs for gas capture at the molecular level, especially SO_2 capture. Damas *et al.* have shown a systematic study of acid- and sour-gas mitigation alternatives (SO_2, CO_2 and H_2S) by using ILs through DFT simulations, which mainly focuses on imidazolium cation based ILs.[17] In this presented work, we broadened the study that was conducted by Damas *et al.* by including other cations such as piridinium or cholinium cations in combination with anions such as bis(trifluorosulfonyl)imide, triflate, or tetrafluoroborate as shown in Table 1 and Fig. 1.

In our opinion, the analysis of those ILs with high efficiency for SO_2 capture through DFT tools should be a good starting

[a] *Department of Chemistry, University of Burgos, 09001 Burgos, Spain. E-mail: sapar@ubu.es*
[b] *Department of Chemical Engineering, Qatar University, P.O. Box 2713, Doha, Qatar*

† Electronic supplementary information (ESI) available. See DOI: 10.1039/c5cp00076a

Table 1 The selected family of ionic liquids studied in this work along with their estimated Henry's Law constants of SO_2 (K_H) at 303 K predicted using the COSMO-RS method

No.	Cation	Anion	Labelling	$K_H \times 10^{-5}$/Pascal
1	1-Ethyl-3-methylimidazolium	Tetrafluoroborate	[EMIm][BF_4]	3.69
2	1-Butyl-3-methylimidazolium	Tetrafluoroborate	[BMIm][BF_4]	3.55
3	1-Hexyl-3-methylimidazolium	Tetrafluoroborate	[HMIm][BF_4]	3.47
4	1-Methyl-3-octylimidazolium	Tetrafluoroborate	[OMIm][BF_4]	3.35
5	1-Butylpyridinium	Tetrafluoroborate	[BPy][BF_4]	3.72
6	1-Butyl-3-methylpyridinium	Tetrafluoroborate	[B3MPy][BF_4]	2.96
7	1-Butyl-4-methylpyridinium	Tetrafluoroborate	[B4MPy][BF_4]	2.96
8	1-Butyl-3-methylimidazolium	Hexafluorophosphate	[BMIm][PF_6]	2.76
9	1-Hexyl-3-methylimidazolium	Hexafluorophosphate	[HMIm][PF_6]	2.65
10	1-Methyl-3-octylimidazolium	Hexafluorophosphate	[OMIm][PF_6]	2.61
11	1-Butylpyridinium	Hexafluorophosphate	[BPy] [PF_6]	2.79
12	1-Butyl-3-methylpyridinium	Hexafluorophosphate	[B3MPy][PF_6]	2.47
13	1-Butyl-4-methylpyridinium	Hexafluorophosphate	[B4MPy][PF_6]	2.46
14	1-Ethyl-3-methylimidazolium	Diethylphosphate	[EMIm][Et_2PO_4]	4.73
15	1,3-Dimethylimidazolium	Dimethylphosphate	[DMIm][Me_2PO_4]	4.07
16	Choline	Dihydrogenphosphate	[CH][H_2PO_4]	6.29
17	1-Ethyl-3-methylimidazolium	Ethylsulfate	[EMIm][$EtSO_4$]	4.63
18	1-Ethyl-3-methylimidazolium	Hidrogensulfate	[EMIm][HSO_4]	6.45
19	1-Ethyl-3-methylimidazolium	Acetate	[EMIm][Ac]	3.85
20	Ethylammonium	Nitrate	[$EtNH_3$][NO_3]	6.37
21	Triethylsulfonium	Bis[(trifluoromethyl)sulfonyl]imide	[Et_3S][NTf_2]	3.52
22	1-Ethyl-3-methylimidazolium	Bis[(trifluoromethyl)sulfonyl]imide	[EMIm][NTf_2]	3.63
23	1-Methyl-3-propylimidazolium	Bis[(trifluoromethyl)sulfonyl]imide	[MPIm][NTf_2]	3.54
24	1,2-Dimethyl-3-propylimidazolium	Bis[(trifluoromethyl)sulfonyl]imide	[DMPIm][NTf_2]	3.19
25	1-Butyl-3-methylimidazolium	Bis[(trifluoromethyl)sulfonyl]imide	[BMIm][NTf_2]	3.50
26	1-Butyl-2,3-dimethylimidazolium	Bis[(trifluoromethyl)sulfonyl]imide	[BDMIm][NTf_2]	3.18
27	1-Hexyl-3-methylimidazolium	Bis[(trifluoromethyl)sulfonyl]imide	[HMIm][NTf_2]	3.50
28	1-Hexadecyl-3-methylimidazolium	Bis[(trifluoromethyl)sulfonyl]imide	[HdMIm][NTf_2]	3.69
29	1-Allyl-3-methylimidazolium	Bis[(trifluoromethyl)sulfonyl]imide	[AMIm][NTf_2]	3.56
30	1-Methyl-1-propylpyrrolidinium	Bis[(trifluoromethyl)sulfonyl]imide	[MPPyr][NTf_2]	3.39
31	1-Butyl-1-methylpyrrolidinium	Bis[(trifluoromethyl)sulfonyl]imide	[BMPyr][NTf_2]	3.36
32	1-Methyl-1-propylpiperidinium	Bis[(trifluoromethyl)sulfonyl]imide	[MPPipe][NTf_2]	3.33
33	1-Butylpyridinium	Bis[(trifluoromethyl)sulfonyl]imide	[BPy][NTf_2]	3.49
34	1-Butyl-3-methylpyridinium	Bis[(trifluoromethyl)sulfonyl]imide	[B3MPy][NTf_2]	3.29
35	1-Butyl-4-methylpyridinium	Bis[(trifluoromethyl)sulfonyl]imide	[B4MPy][NTf_2]	3.29
36	1-Ethyl-3-methylimidazolium	Triflate	[EMIM][SO_3CF_3]	4.41
37	1-Butyl-3-methylimidazolium	Triflate	[BMIM][SO_3CF_3]	4.20
38	1-Hexyl-3-methylimidazolium	Triflate	[HMIM][SO_3CF_3]	4.17
39	1-Methyl-3-octhylimidazolium	Triflate	[OMIM][SO_3CF_3]	4.11
40	1-Butyl-1-methylpyrrolidinium	Triflate	[BMPyr][SO_3CF_3]	3.57
41	1-Ethyl-3-methylimidazolium	Thiocianate	[EMIM][SCN]	4.17
42	1-Ethyl-3-methylimidazolium	Dicyanamide	[EMIM][DCA]	4.30
43	1-Butyl-3-methylimidazolium	Dicyanamide	[BMIM][DCA]	4.22
44	1-Butyl-1-methylpyrrolidinium	Dicyanamide	[BMPyr][DCA]	2.88
45	1-Ethyl-3-methylimidazolium	Chloride	[EMIM][Cl]	2.01
46	1-Butyl-3-methylimidazolium	Chloride	[BMIM][Cl]	3.42
47	1-Allyl-3-methylimidazolium	Chloride	[AMIM][Cl]	2.87
48	1-Ethyl-3-methylimidazolium	Bromide	[EMIM][Br]	2.24
49	1-Butyl-3-methylimidazolium	Bromide	[BMIM][Br]	3.53
50	1,3-Dimethylimidazolium	Iodide	[DMIm][I]	3.39
51	1-Ethyl-3-methylimidazolium	Iodide	[EMIm][I]	3.03
52	1-Methyl-3-propylimidazolium	Iodide	[MPIm][I]	3.70
53	1-Butyl-3-methylimidazolium	Iodide	[BMIm][I]	4.07
54	1-Hexyl-3-methylimidazolium	Iodide	[HMIm][I]	4.50
55	1-Allyl-3-methylimidazolium	Iodide	[AMIm][I]	4.07

point to shed some light on the main molecular factors related with efficient SO_2 capture. Unfortunately, experimental studies dealing with SO_2 capture by ILs are still scarce and reduced to a small number of selected ionic liquids. A key parameter in the selection of an ionic liquid for SO_2 capture is gas solubility. It is well known that gas solubility in ILs can be predicted based on the COSMO-RS (Conductor-like Screening Model for Real Solvents) method.[18] The COSMO-RS predicts thermodynamics properties of solvents on the basis of uni-molecular quantum chemical calculations for the individual molecules, which provides a good

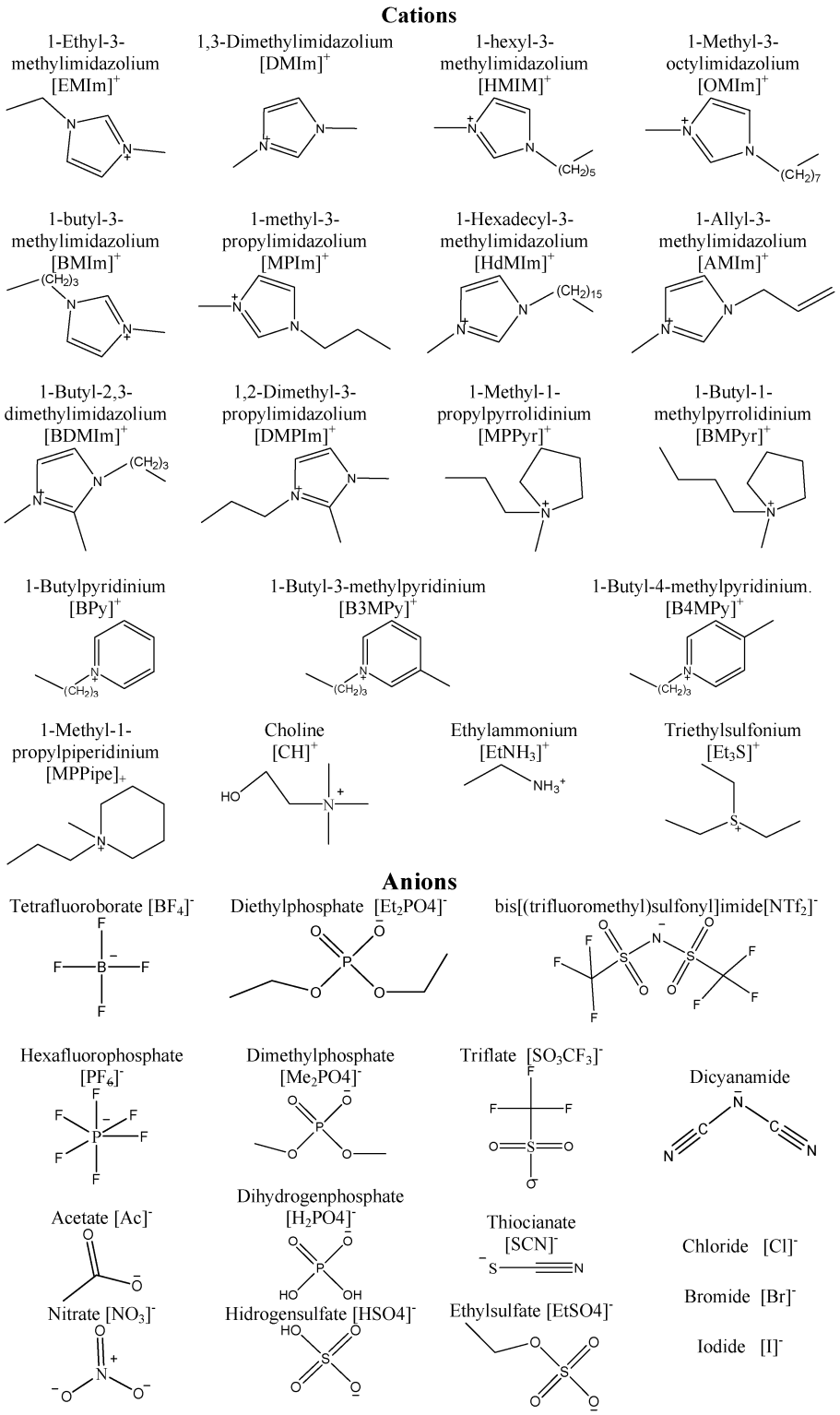

Fig. 1 Chemical structure for the ions involved in the selected family of ionic liquids.

prediction of gas solubility data in ILs without prior experimental knowledge on the compound's properties.[14] Thus, COSMO-RS is able to carry out fast screening on a huge number of ionic liquids, reducing the number of candidates for experimental studies, which also reduces try-and-error attempts and economical and temporal cost. Consequently, the COSMO-RS method was firstly used to carry out a quick screening on a big matrix of ILs. Then, an in-depth study of those ILs, which are expected to provide high SO_2 solubility according to the COSMO-RS method, from a molecular point of view was done using DFT tools. The combination

of first screening to select efficient ILs for SO_2 capture using COSMO-RS analysis along with DFT analysis on the most adequate ILs have allowed us to obtain information about structure *vs.* property relations that control SO_2 solubility in ILs, which is crucial for the rational design of task-specific ILs for SO_2 absorption.

2. Theoretical methodology

2.1. COSMO-RS method

Four different approaches can be performed to describe ionic liquids according to the COSMO-RS method. According to Palomar *et al.*, these approximations are labelled $[C + A]_{GAS}$, $[C + A]_{COSMO}$, $[CA]_{GAS}$ and $[CA]_{COSMO}$.[14] The [C + A] model uses isolated ions to simulate ionic liquids systems, while ion-paired structures are used in [CA]. System optimizations can be carried out in gas-phase using quantum chemistry methods (GAS subscript), or the continuum solvation COSMO model (COSMO subscript). The $[C + A]_{GAS}$ approach (*i.e.* independent ionic structures optimized in the gas phase) predicts gas solubility data in slightly better agreement with the experiments. Palomar *et al.* also concluded that all COSMOS-RS approaches provide similar good capability to predict Henry's law constants for ionic liquid. Nonetheless, the $[C + A]_{GAS}$ model allows us to perform analysis with a reduced computational time, since only optimized ion structures in the gas phase are needed, which is especially useful for screening purposes.

The $[C + A]_{GAS}$ model was employed in this work, which is based on two main steps: (i) quantum chemical optimization for the molecular involved species and (ii) COSMO-RS statistical calculations. Firstly, the isolated ions and SO_2 were optimized at the B3LYP/6-311+G(d,p) level using Gaussian 09 (Revision D.01) package,[19] which was also instructed to provide the COSMO files. For these structures, COSMO files were calculated at the BVP86/TZVP/DGA1 theoretical level and used as input in the COSMOthermX program[18] to estimate Henry's law constants. The COSMO-RS model parameterization used for all calculations was BPTZVPC21-0111.

In this work, Henry's law constants (K_H) for SO_2 were selected as a measure of absorbing capability. Henry's constants are directly calculated by COSMOthermX code. The details of theory of COSMO-RS can be found in the original work of Klamt *et al.*[18] Briefly, Henry's law constants can be defined as the ratio between the liquid phase concentration of SO_2 and its partial vapour pressure in the gas phase:

$$K_H = P_i/x_i = \gamma_i^{\infty} P_i^S \quad (1)$$

where P_i and x_i are the partial vapour pressure of a compound i (SO_2 in our study) in the gas phase and its molar fraction in the liquid. γ_i^{∞} is the activity coefficient of the compound at infinite dilution, and P_i^S is the saturated pure compound vapor pressure of the gas. Those parameters are directly provided by the COSMOthermX code.

2.2. DFT simulations

Systems composed by one isolated molecule (*i.e.* isolated ions and SO_2) up to the system composed by both ions and SO_2 were optimized. Optimized minima were checked through their vibrational frequencies. For those simulations wherein two or more molecules are present, different starting points were employed in order to study different relative dispositions, focusing our attention on the disposition of minimal energy. All these calculations were carried out using a B3LYP-D2 functional. B3LYP[20] has been selected since it has been proven to show appreciable performance over a previously studied wide range of systems,[21] while dispersion corrections (D2) are adequate since we dealt with systems with dispersive interactions such as hydrogen bonds.[22] In addition, other works dealing with the performance of dispersion corrected functionals to study ionic liquid concluded that dispersion correction could significantly decrease mean absolute deviations for binding energies up to 10.0 kJ mol^{-1} or lower in comparison with the MP2 method.[23] All atomic elements, except iodine, were described with the standard Pople basis set 6-311+G(d,p). For iodine, a small core Stuttgart–Dresden–Bonn effective core potential was used (SDB-cc-pVTZ).[24] Interaction energies (BE) related with SO_2 capture were computed as the energy difference between the complex and the sum of the energy of each component. For example, BE for IL$\cdots$$SO_2$ was calculated as:

$$BE = E_{IL-SO_2} - (E_{cat} + E_{ani} + E_{SO_2}) \quad (2)$$

Binding energies were also estimated by considering the IL as a whole (BE′), *i.e.*, the binding energy due to the interaction between the IL and the gas molecule:

$$BE' = E_{IL-SO_2} - (E_{IL} + E_{SO_2}) \quad (3)$$

where E_{IL-SO_2}, E_{cat}, E_{ani}, E_{IL} and E_{SO_2} stand for the energies of IL$\cdots$$SO_2$, cation, anion, IL and SO_2, respectively. For those systems composed of two or more molecules, computed energies were corrected according to the counterpoise method to avoid basis set supper position error (BSSE).[25]

It has been shown that there is a specific charge transfer interaction between SO_2 and the ions.[26] There are different methods to calculate charge distributions, such as the Mulliken method,[27] whose basis set dependence is well known.[28] ChelpG scheme[29] has demonstrated its suitability for ILs.[12,30] Thus, atomic charges were also computed according to both ChelpG and Mulliken schemes. Intermolecular interactions where analyzed in the framework of Bader's theory (Atoms in Molecules, AIM).[31] In this context, intermolecular interactions are characterized through critical points (CP). Although four kind of critical points were obtained, we focused on bond critical points (BCP), which raises the criteria for considering the presence of intermolecular interactions.[31] AIM analysis was carried out with the MultiWFN code.[32] All the above-mentioned calculations were carried out with Gaussian 09 (Revision D.01) package.[19]

3. Results and discussion

3.1. COSMO-RS analysis: selection of the optimal IL family

As said, the first step in our study was the selection of an optimal family of ILs with high SO_2 solubility. The SO_2 absorption capacities were evaluated in terms of Henry's law constants

(K_H) predicted according to the COSMO-RS method. COSMO-RS is a predictive method for thermodynamic equilibrium of fluids, which uses a statistical thermodynamic approach based on the results of uni-molecular quantum chemical calculations. The efficiency of COSMO-RS to predict the solubility behaviour of different solutes in ILs was evaluated by comparing both the experimental and computed (according to the COSMO-RS method) Henry's constants.[14,18,33,34] Although some publications have reported that COSMO-RS systematically overestimates the Henry's constants, it provides a reasonable linear fit between the calculated and experimental values.[14,34]

In this work, COSMO-RS approach has been used to perform a fast screening on SO_2 solubility in ILs. Although several properties, such as σ-surfaces, screening charge density, σ-profiles, and histograms of screening charge can be computed with COSMO-RS, we have focused on Henry's law constants for SO_2 as a measure of absorbing capability. For this, K_H (at 303 K) was estimated for a matrix of ≃7600 ILs formed through a combination of cations based on imidazoluim, piperidinium, choline, ammonium cations paired with anions such as halogens, phosphates, tetrafluoroborate, dicyanamide or bis(trifluorosulfonyl)imide (see Table S1, ESI†). In addition to low Henry's law constants, only those ILs with an adequate viscosity profile for industrial applications as suitable ILs for SO_2 capture were considered. Thus, a set of 55 ILs (see Table 1 and Fig. 1) was selected for a deeper DFT analysis. Table 1 and Fig. 2 gather the computed Henry's law constants of the selected ionic liquids. All selected ILs yield K_H within the range of 2.5×10^5 to 6.5×10^5 Pascal at 303 K. These values are smaller (which means higher solubility) than those reported by González-Miquel *et al.* (of around 30×10^5 Pascal–60×10^5 Pascal) for CO_2 absorption.[35] Then, high efficiency for SO_2 capture can be expected for selected ILs. Note that most of the selected ILs are based on cations such as imidazolium, pyridinium or piperazinium and anions such as $[BF_4]^-$, $[PF_6]^-$, $[NTf_2]^-$ triflate or halides. Then, the combination of these anions would be adequate to design ILs for SO_2 capture with high efficiencies.

3.2. DFT analysis

As a first approximation, SO_2 capture at the molecule level could be related with the strength of the interactions between the ions and the SO_2 molecule. In this work, the interaction strength has been mainly analyzed based on binding energies (BE). Prior to analysis of SO_2 capture by selected ILs, ion···SO_2 and ionic pairs were also briefly assessed. Such information could be useful to rationalize the behavior of IL···SO_2 systems.

3.2.1. Ion···SO_2 systems. Fig. 3 shows computed binding energies (|BE|) for anion···SO_2 interactions. In general, the selected cations provide similar |BE|, whose values lie between 31.70 kJ mol^{-1} ($[BMPyr]^+$) and 42.92 kJ mol^{-1} ($[CH]^+$), except $[EtNH_3]^+$ which yields the largest cation ···SO_2 values, (|BE| = 58.60 kJ mol^{-1}). In concordance with Damas's work, the binding energy for the imizadolium family decreases upon alkyl side chain elongation. In fact, from $[EMIM]^+$ to $[HMIM]^+$, BE varies by only 1.83 kJ mol^{-1}. However, larger alkyl side chains such as $[OMIM]^+$ and $[HdMIM]^+$ lead to a slight increase in BE upon chain elongation. Anion···SO_2 binding energies are, in general, larger than cation···SO_2 binding energies, with values varying between 41.91 kJ mol^{-1} ($[NTf_2]^-$) and 123.37 kJ mol^{-1} ($[H_2PO_4]^-$). Some ions can be classified according to their chemical structure (such as those based on phosphate or sulfate anions). Thus, |BE| of those ones based on dialkyl phosphate slightly decreases (≃4.00 kJ mol^{-1}) upon alkyl chain elongation. The alkyl chain absence in $[H_2PO_4]^-$ leads to |BE| values of 29.12 kJ mol^{-1} which is greater than that of $[Et_2PO_4]^-$. Similar patterns are noted for sulfate-based ions, wherein the presence of an ethyl chain leads to a diminution of 16.48 kJ mol^{-1}. As concerns as halides, |BE| = 52.18 kJ mol^{-1} (in average). In order to compare BE values with experimental data, IL 22 ($[EMIM][NTf_2]$) has been selected as its CO_2 capture performance has been demonstrated experimentally.[11] According to eqn (2), CO_2 capture by IL 22 yields |BE|′ = 36.58 kJ mol^{-1}. This energy could be considered as a low limit, from which higher |BE| would be adequate to provide high SO_2 affinities.

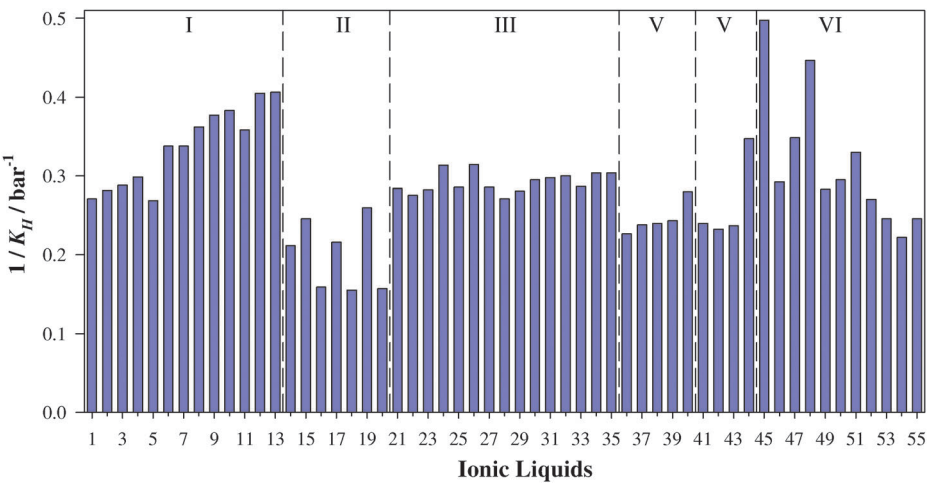

Fig. 2 Inverse of Henry's Law constants of SO_2 in ILs ($1/K_H$) at 303 K predicted using the COSMO-RS method.

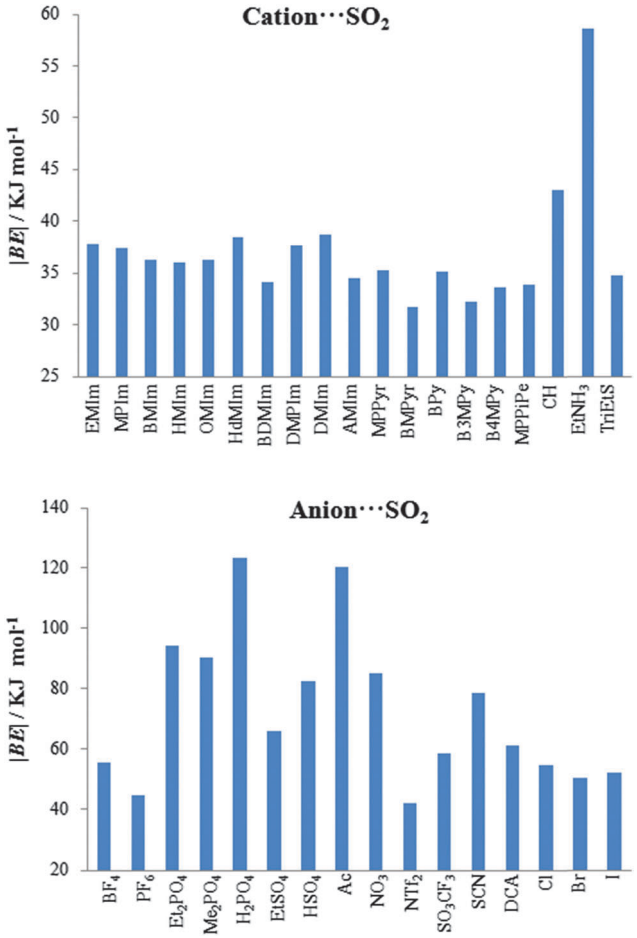

Fig. 3 Computed binding energies (in absolute value, |BE|) of cation···SO_2 (up) and anion···SO_2 (bottom) systems.

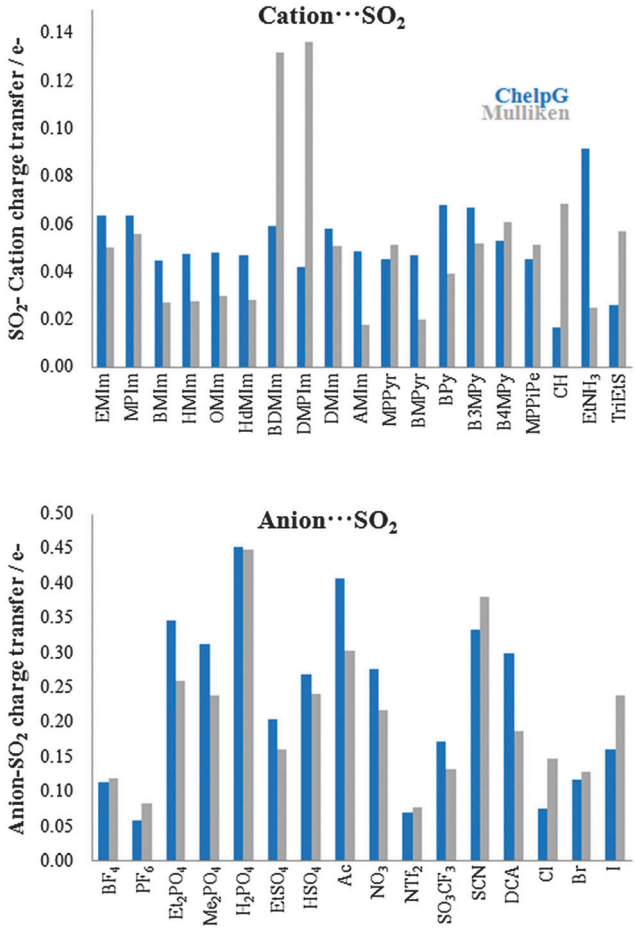

Fig. 4 Charge transfer of cation···SO_2 (up) and anion···SO_2 (bottom) systems.

It has been proven that there is a charge transfer interaction between SO_2 and the anion motif of ILs. This charge transfer interaction is proportional to the anion basicity and plays an important role on the gas adsorption capacity.[26] Fig. 4 collects the charge transfers between the cation/anion and SO_2 molecule. For cation (anion)···SO_2 systems, the total charge over the SO_2 molecule takes positive (negatives) values, which means that charge is transferred from the SO_2 up to the cation (from the anion up to the SO_2). Broadly, charge populations according to the Mulliken scheme are smaller than those computed using the ChelpG model. According to ChelpG (Mulliken) atomic charges, charge transfer between cations and the SO_2 molecule is, on average, 0.05 (0.05) electrons. Thus, van der Waals interactions are one of the main contribution to the |BE| for cation–SO_2 systems, which is in concordance with lower |BE| values than anion–SO_2 systems. Now, the total charge over SO_2 molecule is 0.23(0.21) electrons for anion–SO_2 systems. These higher values are in concordance with greater anion appetency to interact with the SO_2 molecule due to a charge transfer interactions. Fig. 5 shows the relationship between binding energies and charge transfer of anion···SO_2 systems (a similar pattern has not been found for cation···SO_2 systems), which follows a linear behavior for most anions.

3.2.2. Ionic liquids. Fig. 6 gathers computed |BE| of the isolated ionic pair and the charge transfer (CT) between ions according to the ChelpG scheme. Most ILs yield |BE| between 318.99 kJ mol^{-1} (IL 21) and 492.70 kJ mol^{-1} (IL 20), while ILs 25, 29, 31, 33 and 35 provide the smallest values, around 173.09 kJ mol^{-1}. As known, the columbic attraction between opposite charges is the main force between both ions forming the ionic liquid. Even though, other intermolecular forces can also be present. Both the charge transfer and BE follow similar patterns (Fig. 6), *i.e.*, the columbic interaction between both positive and negative charges is one of the main contributions to the binding energy. ILs with the smallest |BE|, *i.e.* IL 25, 29, 31, 33 and 35, are those wherein high charge transfer does not provide high binding energies, which points out that other interactions (such as hydrogen bonds) also represent an important contribution (intermolecular interactions between ions are below described for some ILs). ILs based on halide anions (45–55) show increasing CT with the halide electronegativity. Those effects are stronger from chloride to bromide halides. CTs and binding energies depend on both the cation and anion nature as well. For instance, those ILs based on imidazol cations and $[NTF_2]^-$ anions (except ILs 25 and 29) yield similar |BE| ($\simeq$339.0 kJ mol^{-1}).

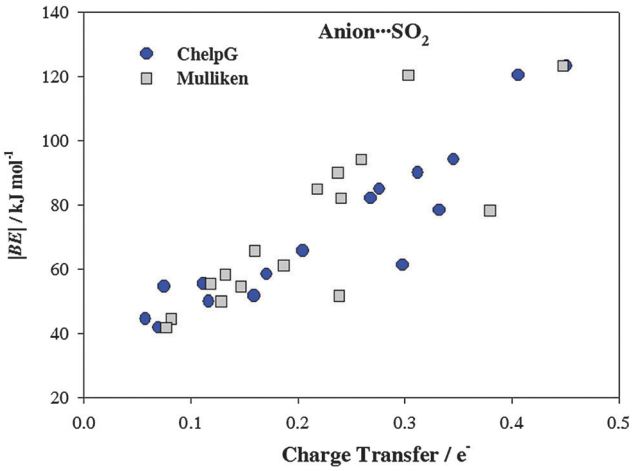

Fig. 5 Binding energies (|BE|) *vs.* charge transfer of anion···SO_2 systems.

3.2.3. SO_2 capture by ionic liquids. Binding energies of IL···SO_2 systems have been used as a measurement of the interaction strength between selected ILs and SO_2 molecule. Fig. 7 collects |BE| (according eqn (2)) of IL···SO_2 systems, which has been decomposed as a sum of the ionic pair, cation···SO_2 and anion···SO_2 contributions. Thus, using the optimized IL···SO_2 geometries, contributions from cation–anion, cation···SO_2 and anion···SO_2 have been also calculated. BE energies were also estimated taking into account the ILs as a whole (eqn (2), |BE′|). All these quantities are also provided in Fig. 7. The largest contribution to the binding energy comes from the interaction between both ions. For an easier comparison, this contribution has been also represented in Fig. 6. For most ILs, the SO_2 molecule only induces a scarce weakening on the interaction between ions (lower |BE|). However, ILs with the lowest |BE| in the absence of SO_2 (ILs 25, 29, 31, 33 and 35, see Fig. 6) are those wherein the SO_2 molecule steers to a strengthening on the interaction between ions. This is due to the phenomena that the new arrangement between ions of SO_2 improves the interaction between both ions and their interactions with the gas molecule, which is described in detail below.

Regarding ion···SO_2 contributions, cation···SO_2 one is, in general, much lower than anion···SO_2 contributions. Even if, the behavior of both ion···SO_2 contributions and its relationship with |BE|′ depends on the analyzed IL. For instance, anion···SO_2 contributions present similar values to |BE′| for ILs 1–6 (based on tetrafluoroborate anion) and 45–55 (based on halides), *i.e.*, anion···SO_2 interactions stand for the main contribution to the total binding energies of these IL–SO_2 systems. Hence, for those ILs based on $[BF_4]^-$ (1–6) and halide (45–55) anions, the SO_2 adsorption process is mainly governed by the anion. For ILs based on triflate, thiocianathe or dicyanamide (ILs 36–44), the sum of both ion···SO_2 contribution yields similar values of |BE′|. In consequence, the SO_2 capture using ILs 36–44 would be guided by both ions. Based on average values, binding energies of cation/anion–SO_2 systems (Fig. 3) yield values $\simeq$37.09 kJ mol^{-1}/72.37 kJ mol^{-1}. However, cation/anion···SO_2 contributions to the binding energy (Fig. 7) are of around 13.94 kJ mol^{-1}/52.03 kJ mol^{-1}. For both ions, interaction energies reduce $\simeq$21.9 kJ mol^{-1} due to the presence of the paired ion. Ions became less negative, since they transfer charge up to both the cation and SO_2 molecule. However, both ions strongly interact between them, hindering cation/anion···SO_2 interactions. Afresh, this general trend depends on the selected family. For example, for $[BF_4]^-$/$[Cl]^-$/$[Br]^-$/$[I]^-$ anion |BE| = 55.45 kJ mol^{-1}/54.64 kJ mol^{-1}/50.07 kJ mol^{-1}/51.83 kJ mol^{-1}, while anion–SO_2 contributions to the total |BE′| for ILs 1–6 (which are those based on tetrafluoroborate anion) are $\simeq$69.28 kJ mol^{-1}, and $\simeq$90.07 kJ mol^{-1} for those ILs based on halides (45–55). As seen above, anion···SO_2 interactions are mainly ruled by the anion···SO_2. Both factors point out that the CT between both ions would increase anion basicity, as well as its interaction strength with the SO_2 molecule. Bearing in mind

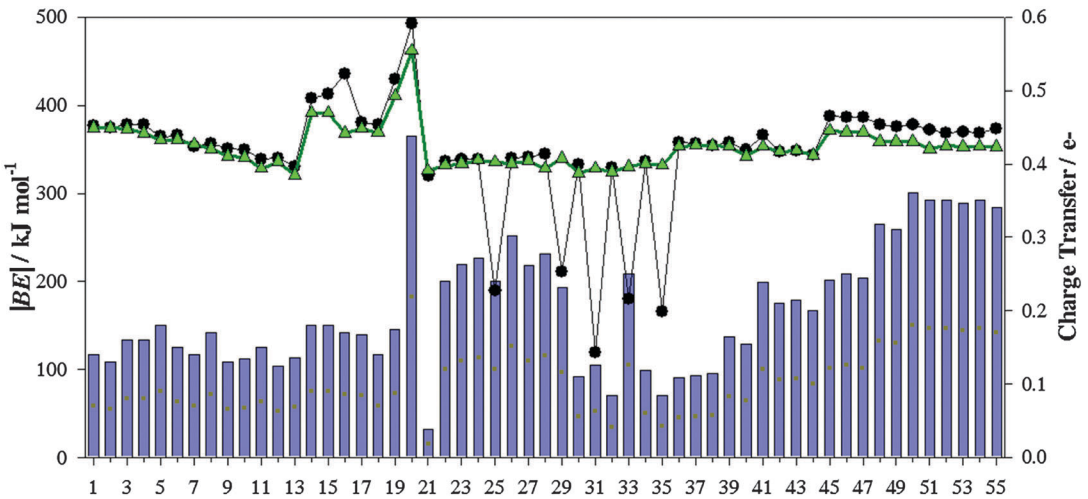

Fig. 6 Computed binding energies (in absolute value, |BE|) of ionic pairs (black line), along charge transfer computed according to the ChelpG scheme (blue bar). Binding energies of ionic pairs using their geometries in the presence of SO_2 are also collected (green line).

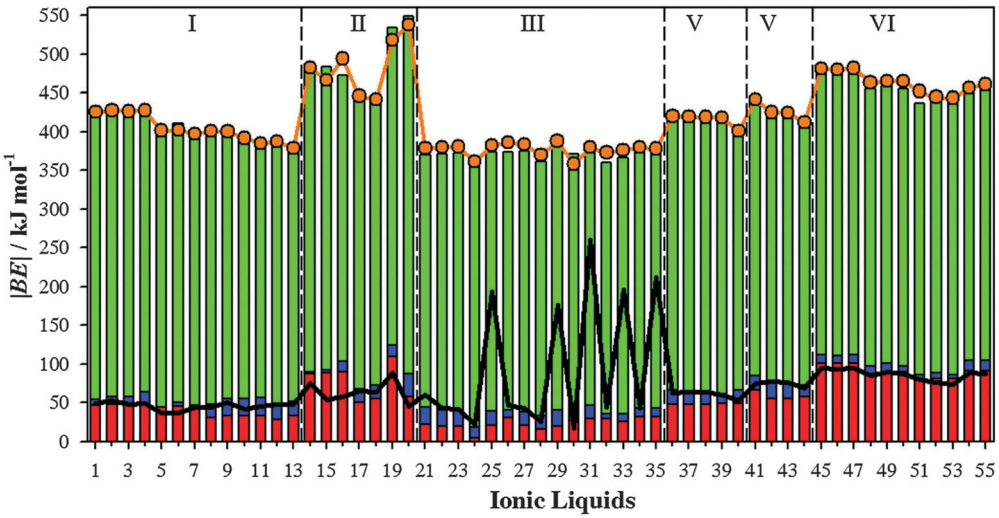

Fig. 7 Computed binding energies (in absolute value, |BE|) of ILs···SO_2 (orange line), along anion···SO_2 contributions (red bar), cation···SO_2 (blue bar) and cation···anion (green bar). Computed binding energies of ILs···SO_2 considering the IL as a whole are also collected (black line).

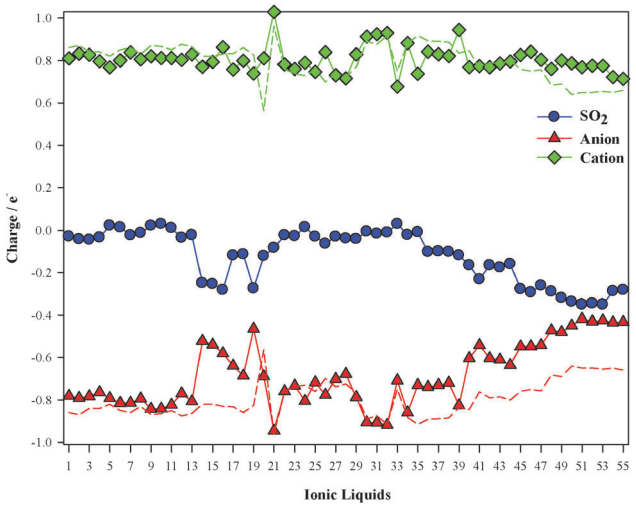

Fig. 8 Computed charge over SO_2 (blue), cation (green) and anion (red) according to the ChelpG scheme. Dotted lines correspond to ion charge for isolated ILs.

a value of around 36.0 kJ mol^{-1} (estimated for CO_2 capture by [EMIM][Tf_2N] IL) as a low limit, almost ILs yield larger values, $|BE'| \simeq 45.0$ kJ mol^{-1}. According to these raised values, an efficient SO_2 capture can be expected. Once more, ILs 25, 29, 31, 33 and 35 do not follow the general trend, since their binding energies despising ionic contribution ($|BE'|$) are much larger than the sum of both ion···SO_2 contributions.

Total charges over both ions and the SO_2 molecule are displayed in Fig. 8. The gas usually gets a negative charge, *i.e.*, there is a charge transfer for the anion up to the SO_2 molecule. Charge populations over both ions for ILs in the absence of SO_2 are also included in Fig. 8. According to the ChelpG scheme, cationic charges slight vary due to the SO_2 molecule, while anionic charges suffer drastic lessening due to the charge transfer up to the SO_2 molecule.

In short, anion···SO_2 interactions play an important role in SO_2 capture by ILs. When both ions are considered, anion···SO_2 strengths will be affected by cation–anion interactions. We have defined the binding energies of IL–SO_2 systems (BE, according eqn (2)) as a function of the BE of ion–SO_2 systems (Section 3.2.1. and Fig. 3) and ionic pairs (Section 3.2.2. and Fig. 6):

$$BE_{IL-SO_2} = (aBE_{CAT-SO_2})^x + (bBE_{ANI-SO_2})^y + (cBE_{IL})^z \quad (4)$$

where BE_{IL-SO_2}, BE_{CAT-SO_2}, BE_{ANI-SO_2}, BE_{IL} are the binding energies of the IL–SO_2, cation–SO_2, anion–SO_2 and anion–cation systems, respectively, while a, b, c, x, y and z are adjustable parameters. Fig. 9a plots the results of a statistical analysis after expressing BE_{IL-SO_2} according to eqn (4). Fig. 9a gathers the data collected for the whole set of ILs. Most of them yield a linear behavior between BE_{IL-SO_2} estimated from the IL–SO_2 optimized systems ($BE_{IL-SO_2,DFT}$) and those ones after the fit of eqn (4) ($BE_{IL-SO_2,Statistical}$). Hence, the total binding energy of IL–SO_2 systems, which takes into account both anion–cation and anion–SO_2 interactions, could be directly obtained through the optimization of ion···SO_2 systems and ILs. The fit yields $R^2 = 0.6772$ and medium deviation (MD) = 3.20 kJ mol^{-1}, which could be considered an acceptable value despite the variety in the chemical structure of the selected ionic liquid. The largest errors correspond to ILs 25, 29, 31, 33 and 35 ($|BE_{IL-SO_2,Statistical}| \simeq 360.0$ kJ mol). As seen above, those ILs suffered and strengthening of the interaction between ions due to the presence of the SO_2 molecule occurred. According to eqn (4), no important differences on binding energies for ILs are expected upon SO_2 presence. On the other hand, IL 20 ($|BE_{IL-SO_2,Statistical}| = 578.34$ kJ mol) is based on $[EtNH_3]^+$ cation. $[EtNH_3]^+$–SO_2 provided the highest binding energy among all studied cations. According with a parameter ($a = 1.28 \times 10^{-16}$), contribution from BE_{CAT-SO_2} is close to zero. Hence, the above expression is only applicable to those ILs wherein the anion plays the main role on SO_2 capture and for those ILs which do

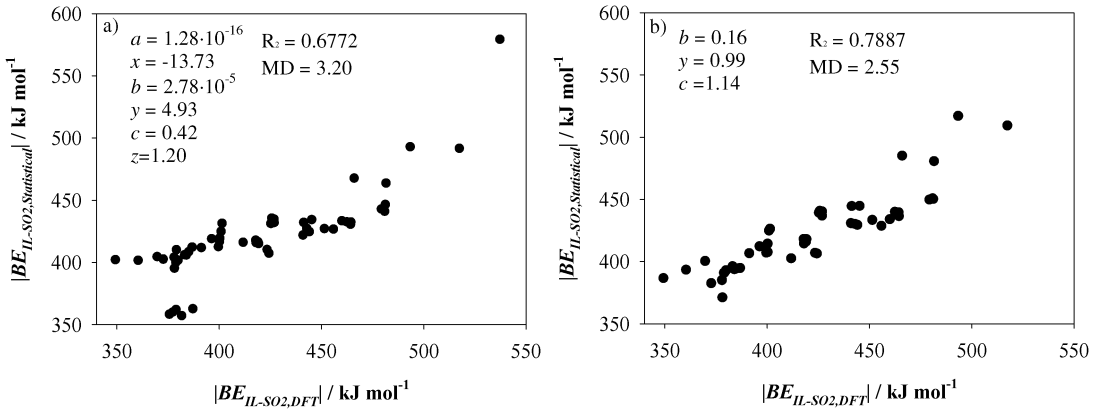

Fig. 9 Results from the fit of BE_{IL-SO_2} according to eqn (4) and (5).

not suffer important geometrical arrangements in the presence of the gas molecule. Note that the z parameter is close to one. As a result, we defined eqn (4) based only on BE_{ANI-SO_2} and BE_{IL}. $BE_{IL-SO_2,Statistical}$ as follows:

$$BE_{IL-SO_2,Statistical} = b(BE_{ANI-SO_2})^y + cBE_{IL} \quad (5)$$

The fit was repeated despising ILs 20, 25, 29, 31, 33 and 35. As seen in Fig. 9b, there is a notable improvement in the fit performance with R^2 = 0.7887 and MD = 2.55 kJ mol^{-1}. It could be concluded that SO_2 capture by ILs is mainly governed by ILs, while interactions between ions are also an important parameters. Since BE between ions is much higher than anion–SO_2 ones, BE_{IL} grants the most important contribution to $BE_{IL-SO_2,Statistical}$. Then, for those ILs with similar BE_{IL}, the efficiency in SO_2 capture will be ruled by the anion. In addition, eqn (5) allows estimating BE_{IL-SO_2} only through the optimization of anion–SO_2 and cation–anion systems, which can be considered a useful insight into the rational design of ILs for SO_2 capture.

3.2.4. Representative ionic liquids for SO_2 capture. Up to now, properties for IL$\cdots SO_2$ interactions have been analyzed for the whole family of selected ILs based on binding energies. As seen, the SO_2 absorption capacity is often governed by anion$\cdots SO_2$ interactions, although cations have also an important role. Even though, cation–SO_2 contributions to the total |BE′| are always lower than cation–SO_2 binding energies, while this general trend was not found for anion$\cdots SO_2$ contributions. For instance, anion$\cdots SO_2$ contributions to the total |BE′| for ILs (1–4, which are based on imidazolium cations paired with tetrafluoroborate anion) are higher than binding energies for anion–$[BF_4]^-$ systems, while the opposite trend was noted for ILs 22–29 (also based on imidazol derived cations, but paired with the $[NTf_2]^-$ anion). In addition, a statistical analysis has shown that BE of IL–SO_2 systems mainly depends on anion–SO_2 and cation–anion interactions. The diversity in the nature of both ions forming the family of studied ILs hinders the search of structure–property relationships. Therefore the IL family has been divided into six sets (labelled as I–VII, see Fig. 2 and 7), wherein ILs within the same sets have similar features regarding the chemical structure of their ions. For each one, the most representative ILs have been selected, whose intermolecular interactions where analyzed within the context of the AIM theory to obtain some information on the SO_2 capture mechanism at the nanoscopic level.

Set I (ILs 1–13) includes ILs based on imidazolium ($[Im]^+$) or pyridinium ($[Py]^+$) cations paired with $[BF_4]^-$ or $[PF_6]^-$ anions. ILs based on imidazolium and $[BF_4]^-$ (ILs 1–4) yields similar $K_H \simeq 3.6 \times 10^5$ Pascal and $|BE'| \simeq 49.65$ kJ mol^{-1}. $[Im][PF_6]$ based ILs (8–10) render smaller K_H ($\simeq 2.7 \times 10^5$ Pascal); however this improvement in K_H is not observed on |BE′| ($\simeq$45.19 kJ mol^{-1}). For pyridinium based ILs (5–7 and 11–13) The replacement of $[Im]^+$ by $[Py]^+$ does not lead to important changes on K_H and |BE′|. Though, the alkyl chain length in the cation, as well as the presence of $[BF_4]^-$ or $[PF_6]^-$ anions have an effect of thermophysical properties such as viscosity or density.[30,36] ILs included in set I would provide similar SO_2 capture efficiency (based on K_H and |BE′| values). As a matter of fact, several papers highlight the effect on macroscopical properties as a function of the selected ions elsewhere.[30,36,37] In order to discuss the effects on different ions at the molecular level, besides previously described parameters, the interaction mechanisms of [BMIm][BF_4] (IL 2), [BMIm][PF_6] (IL 8), [B4MPy][BF_4] (IL 7) and [B4MPy][PF_6] (IL 13) have been deeply analyzed as representative compounds of this set. Intermolecular interactions were localized and featured through the AIM theory (we have focused on electronic density values, ρ, for the main intermolecular interactions). Fig. 10 plots their optimized structures in the presence of the SO_2 molecule (optimized geometries for isolated ILs are not represented since the presence of SO_2 does not carry out important changes on the relative disposition between ions), whereas bond length and AIM features of intermolecular interactions are reported in Table 2. In the absence of the SO_2 molecule, several anion–cation interactions are established. The main interactions are formed between F and H in position 2 of the imidazolium/pyridinium ring, whose d (intermolecular distance) and ρ are $\simeq$2.240 and 0.0140 a.u., respectively. In this sense, it is well known that the main interaction in imidazilium based ILs is carried out through the H atom in position 2.[17] The presence of the SO_2 molecule leads to an intermolecular distance

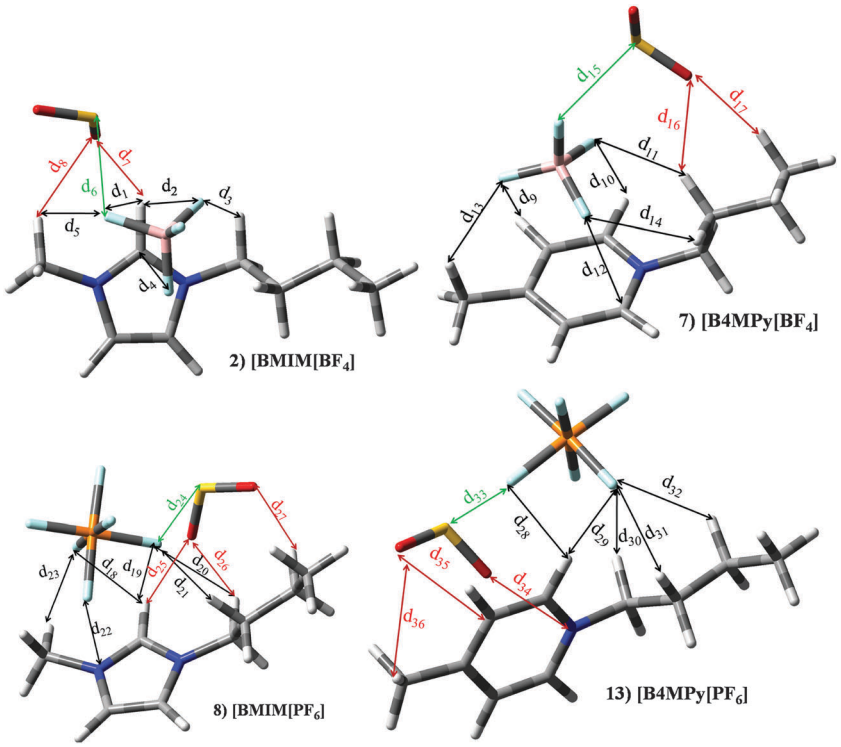

Fig. 10 Optimized geometries of [BMIm][BF_4] (2), [B4MPy][BF_4] (7), [BMIm][PF_6] (8) and [B4MPy][PF_6] (13) in the presence of the SO_2 molecule. Main intermolecular interactions are also displayed. Atom colour code: C (gray), oxygen (red) sulphur (yellow), hydrogen (white), nitrogen (blue), boron (pink), phosphorous (orange) and fluorine (light blue). See Table 2 for a more detailed description on intermolecular interactions.

elongation and electronic density decrease, in concordance with lower |BE| of ILs using their geometries in the presence of SO_2. As seen below, this effect is also noted for almost all ILs under study. Anion–SO_2 interactions are mainly characterized by a BCP between F and S, labeled as d_6, d_{15}, d_{24} and d_{33} for ILs 2, 7, 8 and 13, respectively, whose ρ are 0.0273 a.u., 0.0189 a.u., 0.0135 a.u., 0.0092 a.u., respectively. Similar patterns are noted for anion–SO_2 contribution to the total binging energies (Fig. 7). Cation–SO_2 interactions take place through O (SO_2) and H (cation). These H are mainly located on the alkyl side chain. For ILs based on $[B3MPy]^+$/$[B4MPy]^+$ based ILs (6/7 and 12/13), the presence of methyl chain in position 3/4 brings slight improvement on K_H and BE with respect to $[BPy]^+$. This methyl group in position 3/4 allows an additional intermolecular interaction (*e.g.*, d_{13} for IL 7) with SO_2, which is absent for $[BPy]^+$.

ILs based on phosphate, sulfate, acetate or nitrate anions are located in set II. Most of them are also based on $[EMIm]^+$ cation. Interaction energies of anion$\cdots SO_2$ systems (see Fig. 3); $[Et_2PO_4]^-$ (99.24 kJ mol^{-1}), $[EtSO_4]^-$ (65.75 kJ mol^{-1}), $[Ac]^-$ (120.47 kJ mol^{-1}) and $[NO_3]^-$ (85.06 kJ mol^{-1}), are larger than those estimated for $[EMIm]^+$ (33.77 kJ mol^{-1}) and $[EtNH_3]^+$ (58.60 kJ mol^{-1}) cations. Analogous behaviour is noted for both ion$\cdots SO_2$ contribution to the binding energy, *i.e.*, anion$\cdots SO_2$ > cation$\cdots SO_2$. Nevertheless, the sum of both contributions is higher than |BE′| (see Fig. 7). In concordance with |BE| computed for cation/anion$\cdots SO_2$, anion$\cdots SO_2$ contribution to the total BE is larger. Within this set we have focused on $[EMIm][Et_2PO_4]$ (14), $[EMIm][EtSO_4]$ (17) and [EMIm][Ac] (19) ILs. A detailed analysis of $[CH][H_2PO_4]$ at the molecular level and their application for SO_2 capture will be studied in a separate work in the future. The structures of $[EMIm][Et_2PO_4]$ (14), $[EMIm][EtSO_4]$ (17) and [EMIm][Ac] (19) in the presence and absence of SO_2 are reported in Fig. 11. $[EtNH_3][NO_3]$ (20) IL has been also selected to obtain some insight up to the behaviour of this IL. In the absence of the SO_2 molecule, the main interaction between imidazolim cation and the corresponding anion is carried out by a hydrogen bond between the O atom (anion) and H in position 2 of the imidazolium ring (labelled d_1, d_8 and d_{16} for ILs 14, 17 and 19 respectively). Again, the presence of the SO_2 molecule brings a diminution of the interaction between both ions. As seen in Fig. 7 for IL 17, contribution from anion$\cdots SO_2$ interaction to the |BE| is larger than cation$\cdots SO_2$ interaction, which agrees with larger ρ values for d_{12} regarding to interaction between cation and SO_2, *i.e.*, d_{13} and d_{14} (similar behaviour can be drawn for ILs 14 and IL19). The SO_2 molecule interacts with the anion through an intermolecular bond between the S and one oxygen atom located in the anion. $[EtNH_3][NO_3]$ (20) presents the highest charge transfer and |BE| between ions in the absence of SO_2 (see Fig. 6). As seen in Fig. 11, there is a proton transfer between ions. In fact, the distance between $[NO_3]^-$ and H (d_{23}) is 1.045 Å, while the distance between N and H (d_{24}) is 1.595 Å. ChelpG charges have shown that such O has an atomic charge of −0.58 (larger than the −0.46 e$^-$ over the other O), while the positive charge over this H is 0.39 (charge over remaining H linked to N is of around 0.26 e$^-$).

Table 2 Intermolecular distances (d) along the electronic density values (ρ) of [BMIm][BF_4] (2), [B4MPy][BF_4] (7), [BMIm][PF_6] (8) and [B4MPy][PF_6] (13) ionic liquids. See Fig. 10 for labeling

	IL		IL···SO_2	
	d/Å	ρ/a.u.	d/Å	ρ/a.u.
2 – [BMIm][BF_4]				
d_1	2.233	0.0143	2.788	0.0076
d_2	2.106	0.0178	2.457	0.0121
d_3	2.502	0.0082	2.502	0.0091
d_4	2.873	0.0101	2.892	0.0102
d_5	2.222	0.0130	2.447	0.0100
d_6			2.531	0.0273
d_7			2.518	0.0087
d_8			2.118	0.0170
7 – [B4MPy][BF_4]				
d_9[a]	2.298	0.0129	2.910	0.0097
d_{10}	2.119	0.0173	2.549	0.0148
d_{11}[a]	2.671	0.0117	2.484	0.0081
d_{12}	2.322	0.0097	2.870	0.0105
d_{13}			2.479	0.0077
d_{14}	2.289	0.0120	2.706	0.0188
d_{15}			2.716	0.0089
d_{16}			2.496	0.0082
d_{17}			2.429	0.0097
8 – [BMIm][PF_6]				
d_{18}	2.406	0.0113	2.421	0.0116
d_{19}	2.320	0.0138	2.607	0.0101
d_{20}	2.413	0.0107	2.701	0.0067
d_{21}[b]	2.479	0.0100	2.315	0.0118
d_{22}	2.698	0.0142	2.803	0.0094
d_{23}	2.488	0.0097	2.648	0.0206
d_{24}			2.652	0.0135
d_{25}			2.209	0.0084
d_{26}			2.535	0.0071
d_{27}			2.548	0.073
13 – [B4MPy][PF_6]				
d_{28}	2.328	0.0116	2.363	0.0128
d_{29}	2.124	0.0167	2.078	0.0181
d_{30}	2.313	0.0113	2.481	0.0145
d_{31}[a]	2.588	0.0114	2.446	0.0095
d_{32}			2.698	0.0057
d_{33}			2.648	0.0092
d_{34}			2.955	0.0065
d_{35}			3.218	0.0059
d_{36}			2.718	0.0058

[a] For isolated IL, this interaction take places between F and H in position 2. [b] For isolated IL, this interaction takes places between F and C in position 2.

This effect is not observed in the presence of the SO_2 molecule. The adsorption of SO_2 by IL 20 is carried out by a strong interaction between SO_2 and the anion (d_{25}), while there are dual interactions between SO_2 and the cation (d_{26} and d_{27}, being the latter the weakness). Once more, a larger electronic density for d_{35} (respect to d_{26}) agrees with the greater contribution from SO_2···interaction to $|BE'|$.

ILs based on the $[NTf_2]^-$ anion (set III) are the largest group, whose $K_H \simeq 3.4 \times 10^5$ Pascal and $|BE'| \simeq 38.45$ kJ mol^{-1} (despising ILs 25, 29, 31, 33 and 35). For ILs 25, 29, 31, 33 and 35, $|BE'|$ is much larger than sum of both ion···SO_2 contributions. Furthermore, ILs 25, 29, 31, 33 and 35 are the only ones whose interactions between ions are strengthened in the presence of the SO_2 molecule (see Fig. 6). The SO_2 brings a rearrangement between ions which improves their mutual interaction and also their interactions with SO_2. To obtain information about this fact, we have focused on IL [BMIm][NTf_2]. Optimized geometries as well as the main results from intermolecular interaction

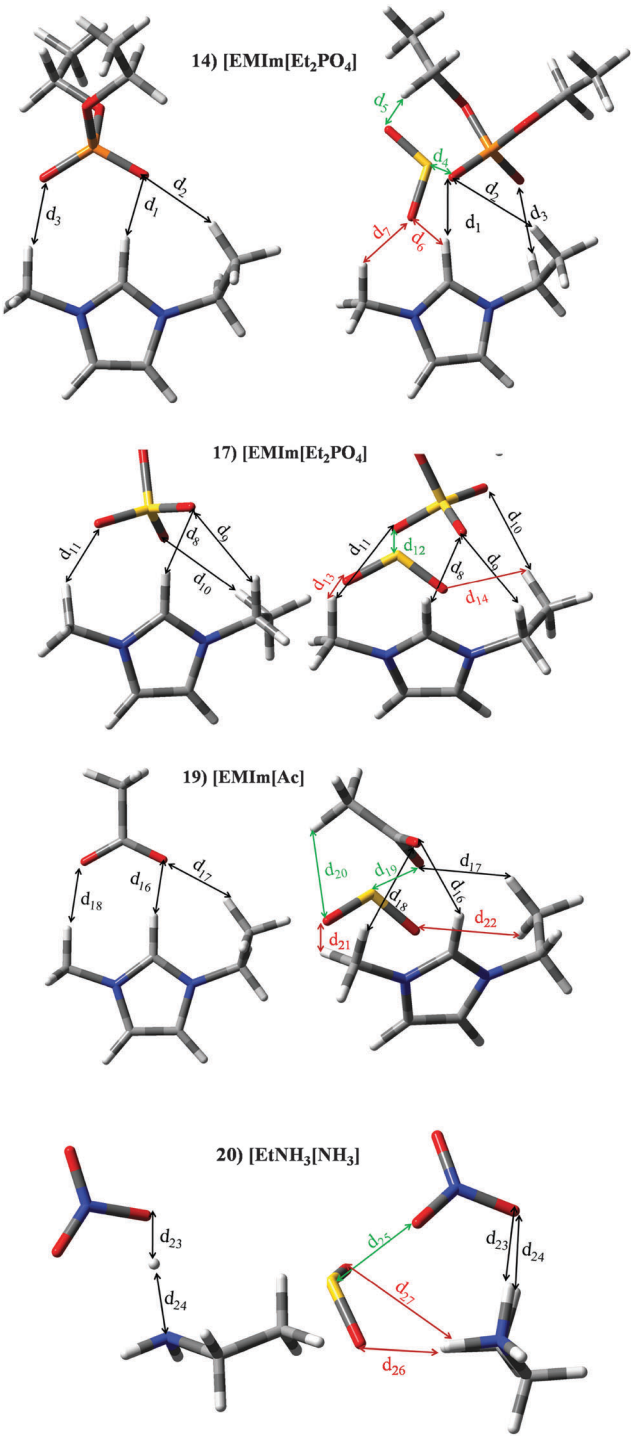

Fig. 11 Optimized geometries of [EMIm][Et_2PO_4] (14), [EMIm][$EtSO_4$] (17), [EMIm][Ac] (19) and [$EtNH_3$][NO_3] (20). Main intermolecular interactions are also displayed. Atom colour code: C (gray), oxygen (red) sulphur (yellow), hydrogen (white), nitrogen (blue)and phosphorous (orange). See Table 3 for a more detailed description on intermolecular interactions.

Table 3 Intermolecular distances (d) along the electronic density values (ρ) of [EMIm][Et_2PO_4] (14), [EMIm][$EtSO_4$] (17), [EMIm][Ac] (19) and [$EtNH_3$][NO_3] (20). See Fig. 11 for labeling

	IL		IL···SO_2	
	d/Å	ρ/a.u.	d/Å	ρ/a.u.
14 – [EMIm][Et_2PO_4]				
d_1	1.756	0.0299	1.793	0.0369
d_2	2.304	0.0120	2.780	0.0194
d_3	1.962	0.0253	2.119	0.0064
d_4			2.238	0.0575
d_5			2.510	0.0088
d_6			2.578	0.0087
d_7			2.242	0.0144
17 – [EMIm][$EtSO_4$]				
d_8	2.055	0.0231	2.052	0.0225
d_9	2.510	0.0095	2.500	0.0096
d_{10}	2.417	0.0103	2.513	0.0087
d_{11}	2.184	0.0159	2.555	0.0082
d_{12}			2.243	0.0396
d_{13}			2.419	0.0109
d_{14}			2.444	0.0081
d_{15}			2.576	0.0059
19 – [EMIm][Ac]				
d_{16}	1.654	0.0278	2.110	0.0205
d_{17}	2.352	0.0109	2.491	0.0097
d_{18}	2.002	0.0240	2.427	0.0104
d_{19}			2.189	0.0658
d_{20}			2.667	0.0077
d_{21}			3.665	0.0128
d_{22}			2.583	0.0082
20 – [EMIm][NO_3]				
d_{23}	1.596	0.0072	1.639	0.0564
d_{24}	1.045		2.625	0.0078
d_{25}			2.350	0.0454
d_{26}			1.820	0.0328
d_{27}			2.620	0.0074

analysis are collected in Fig. 12 and Table 4. [BMIm][NTf_2] ILs yields five intermolecular interactions (d_1–d_5) between both ions, wherein the one between the N (anion) and the H (cation) is position 2 is the strongest one. Although the same interactions between both ions are found in the presence of the SO_2 molecule, all of them suffer an elongation/decrease on intermolecular distances/electronic density values. SO_2 molecule is able to for two bonds with the anion, *i.e.*, d_6 (S···O) and d_7 (S···F), being the latter much weaker than S···O interaction. Further, two O···H bonds (d_8 and d_9) are noted between SO_2 and cation molecules. Although SO_2 causes a weakening of the interaction between ions (based on electronic density values), it also allows the formation of a cage, with their corresponding cage critical points (CCP). Concretely, two cage critical points (represented as purple points along the *yz* view) are found, whose electronic density is 0.0027 a.u. and 0.0018 a.u. The presence of both CCP points out to a charge delocalization process between different motifs. Results described for this IL could be extrapolated to ILs 29, 31, 33 and 35, *i.e.*, larger |BE′| values and stronger interaction between ions are due to the charge delocalization process. This charge delocalization brings an increase on inter ionic interaction (with respect to isolated IL), and |BE′| is higher than the sum of both ion···SO_2 contributions. Although, CCPs are also

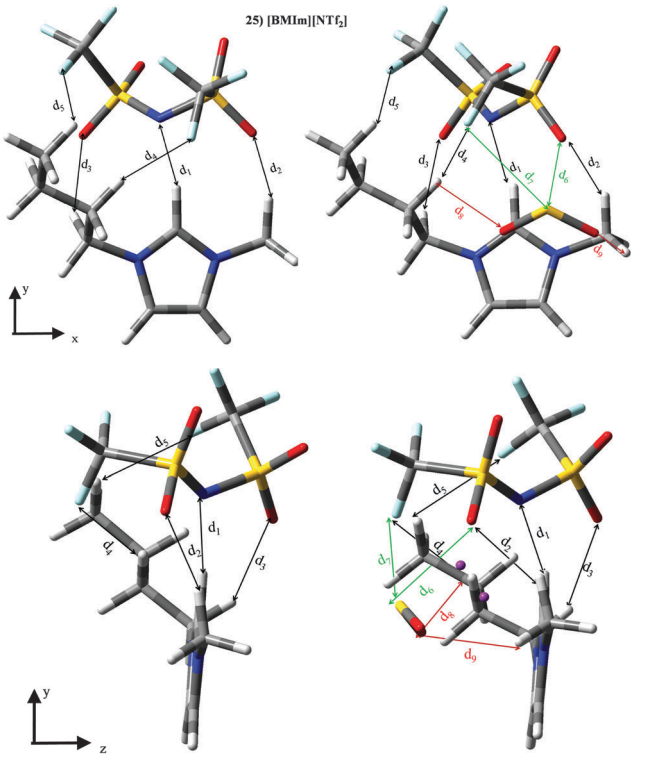

Fig. 12 Optimized geometries of [BMIm][NTf_2] (25), [BMPyr][NTf_2] (31) and [B4MPy][NTf_2] (35). Main intermolecular interactions are also displayed. Atom colour code: C (gray), oxygen (red) sulphur (yellow), hydrogen (white), nitrogen (blue) and phosphorous (orange). See Table 4 for a more detailed description on intermolecular interactions.

Table 4 Intermolecular distances (d) along the electronic density values (ρ) of [BMIm][NTf_2] (25). See Fig. 12 for labeling

	IL		IL···SO_2	
	d/Å	ρ/a.u.	d/Å	ρ/a.u.
25 – [BMIm][NTf_2]				
d_1	1.952	0.0303	2.020	0.0266
d_2	2.186	0.0150	2.419	0.0104
d_3	2.290	0.0130	2.352	0.0115
d_4	2.564	0.0063	2.594	0.0058
d_5	2.553	0.0024	2.623	0.0058
d_6			2.683	0.0218
d_7			3.208	0.0062
d_8			2.739	0.0068
d_9			2.479	0.0099

found for other ILs, they own much lower electronic density values.

ILs based on the triflate anion ($[SO_3CF_3]^-$) are within set IV (IL 36–40). Those ones also based on imidazolium cations (36–39) provide $K_H \simeq 4.22 \times 10^5$ Pascal and $|BE'| \simeq 60.30$ kJ mol^{-1}, which is due to the sum of both ion···SO_2 contributions. [BMPyr][SO_3CF_3] (IL40) yields $K_H = 3.57 \times 10^5$ Pascal and $|BE'| = 51.97$ kJ mol^{-1}, mainly due to the anion···SO_2 contribution. Larger anion···SO_2 contributions (Fig. 7) to the binding energy mimic the previously reported compound for ion···SO_2 binding energies (Fig. 3). Fig. 13 and Table 5 gather optimized geometries and intermolecular

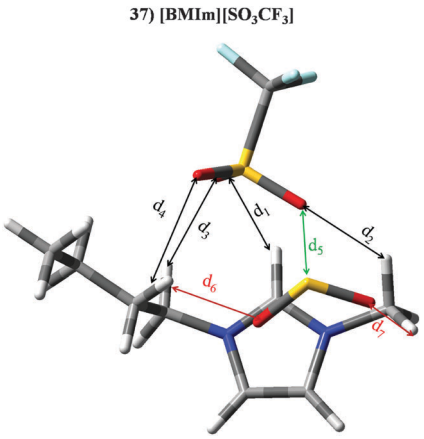

Fig. 13 Optimized geometries of [BMIm][SO_3CF_3] (37) in the presence of SO_2 (similar results are obtained for isolated IL). Main intermolecular interactions are also displayed. Atom colour code: C (gray), oxygen (red) sulphur (yellow), hydrogen (white), nitrogen (blue) and fluorine (light blue). See Table 5 for a more detailed description on intermolecular interactions.

Table 5 Intermolecular distances (d) along the electronic density values (ρ) of [BMIm][SO_3CF_3] (37). See Fig. 13 for labeling

	IL		IL···SO_2	
	d/Å	ρ/a.u.	d/Å	ρ/a.u.
37 – [BMIm][SO_3CF_3]				
d_1	2.025	0.0239	2.184	0.0070
d_2	2.280	0.0130	2.626	0.0109
d_3	2.520	0.0081	2.439	0.0089
d_4	2.594	0.0088	2.544	0.0351
d_5			2.476	0.0096
d_6			2.464	0.0107
d_7			2.451	0.0070

parameters for [BMIm][SO_3CF_3] (37). Results obtained for this IL could be extrapolated for the whole set IV. The main interaction between both ions takes places through O corresponding to the anion and H in position 2 located in the cation (d_1), whose ρ and distances are more affected by the SO_2 molecule, which causes its weakening. However, the remaining interactions are slightly affected by the gas molecule. Thus, binding energy for IL 37 is very similar to contribution from inter ionic interaction to the BE estimated for the IL 37···SO_2 system (see Fig. 6). The adsorption of SO_2 by IL 37 is mainly carried out through O (anion)···S(SO_2) interaction (labelled as d_5). Even if, SO_2 molecule also owns two intermolecular O···H bonds with alkyl H atoms located in the cation (d_6 and d_7). In concordance with ion··· contributions to |BE′|, anion···SO_2 interaction (based on its larger electronic density value) is greater than cation···SO_2 interaction.

Set V (IL 41 44) comprises those ILs whose anions have at least one CN group, *i.e.*, thiocianate ($[SCN]^-$) and dicyanamide ($[DCA]^-$). ILs based on the imidazolium cation (41–43) supply $K_H \simeq 4.23 \times 10^5$ Pascal and |BE′| $\simeq$ 76.21 kJ mol^{-1}, while [BMPyr][DCA] (IL 44) yields $K_H = 2.88 \times 10^5$ Pascal and |BE′| = 68.20 kJ mol^{-1}. Isolated ions provided |BE| = 78.40 kJ mol^{-1} and 61.29 kJ mol^{-1}, while |BE| for imidazolium and [BMPyr] + are $\simeq$ 36.99 kJ mol^{-1} and 31.70 kJ mol^{-1}, respectively. Anew, the trend perceived for the interaction between anions (cation) and SO_2 in the absence of the cation (anion) is also found for both ion···SO_2 contributions to the binding energies. [EMIM][SCN] (41) brings a |BE′| similar to anion···SO_2 contribution, while |BE′| for $[DCA]^-$ based ILs comes from both ion···SO_2 contributions. Fig. 14 and Table 6 reports optimized geometries for [EMIm][SCN] (41), [EMIm][DCA] (42) and [BMPyr][DCA] (44). As expected (in the absence of SO_2), both ions interact with the $[EMIM]^+$ cation through its H in position 2. S and N terminal atoms from $[SCN]^-$ anion are able to interact with these H atoms (d_1 and d_2). Further, the S atom also provides an intermolecular interaction with methyl hydrogen (d_3). Although, $[DCA]^-$ owns two CN groups, only one of them interacts with H in position 2 (d_8), even though two interactions with alkyl H atoms are also found (d_9 and d_{10}). Regarding IL 44, only one N group interacts with the main position provided by the cation (d_{14}), although other intermolecular H bonds (with lower ρ) are also present (d_{15}–d_{18}). According to electronic density values, ionic interactions are stronger for $[SCN]^-$ anion, which agrees with its higher |BE| vales (see Fig. 6). ILs 41, 42 and 44 show similarities regarding to the interactions with the gas molecule. Thus, the main interaction is carried out between one terminal N (anion) and the central S atom (d_5, d_{11} or d_{19} for IL 41, 42 or 44, respectively). Although electronic density for d_5 (0.387 a.u.) is smaller than electronic density for d_{11} and d_{19} ($\simeq$0.423 a.u.), larger charge transfer from the $[SCN]^-$ anion up to the gas (see Fig. 8) agrees with greater $[SCN]^-$···SO_2 contribution in

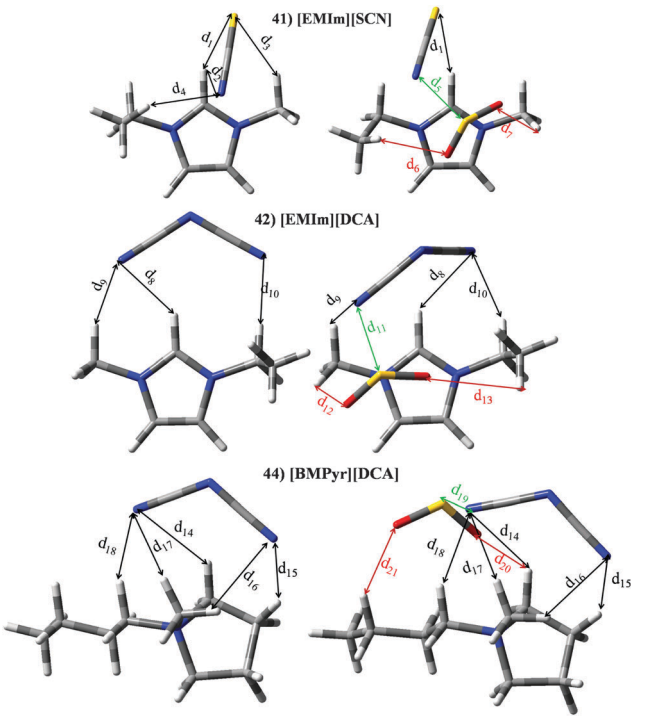

Fig. 14 Optimized geometries of [EMIM][SCN] (41), [EMIM][DCA] (42) and [BMPyr][DCA] (44). Main intermolecular interactions are also displayed. Atom colour code: C (gray), oxygen (red) sulphur (yellow), hydrogen (white), nitrogen (blue) and fluorine (light blue). See Table 6 for a more detailed description on intermolecular interactions.

Table 6 Intermolecular distances (d) along the electronic density values (ρ) of [EMIm][SCN] (41), [EMIm][DCA] (42) and [BMPyr][DCA] (44). See Fig. 14 for labeling

	IL		IL···SO_2	
	d/Å	ρ/a.u.	d/Å	ρ/a.u.
41 – [EMIm][SCN]				
d_1	2.567	0.0152	2.572	0.0141
d_2	2.907	0.0142		
d_3	2.841	0.0092		
d_4	2.532	0.0093		
d_5			2.369	0.0387
d_6			2.506	0.0089
d_7			2.513	0.0107
42 – [EMIm][DCA]				
d_8	2.348	0.0137	2.480	0.0115
d_9	2.180	0.0177	2.395	0.0051
d_{10}	2.161	0.0181	2.535	0.0048
d_{11}			2.431	0.0430
d_{12}			2.376	0.0118
d_{13}			2.630	0.0074
44 – [BMPyr][DCA]				
d_{14}	2.750	0.0084	2.745	0.0088
d_{15}	2.462	0.0106	2.406	0.0097
d_{16}	2.689	0.0075	2.534	0.0117
d_{17}	2.550	0.0104	2.585	0.0103
d_{18}	2.294	0.0143	2.463	0.0105
d_{19}			2.464	0.0105
d_{20}			2.617	0.0103
d_{21}			2.448	0.0088

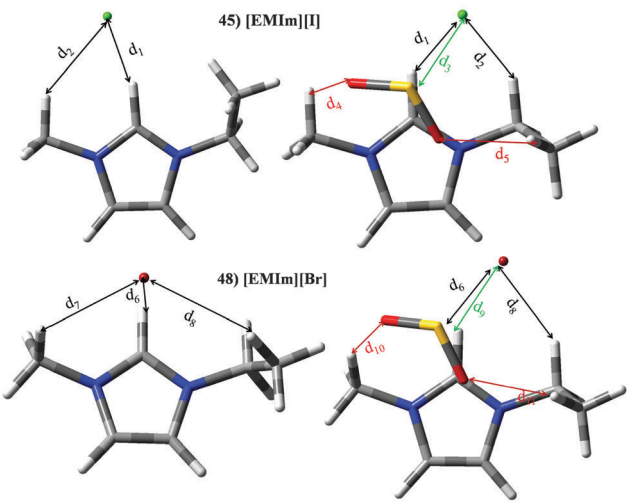

Fig. 15 Optimized geometries of [EMIm][Cl] (45) and [EMIM][Br] (48). Similar geometries are obtained for [EMIM][I] (51). Main intermolecular interactions are also displayed. Atom colour code: C (gray), oxygen (red) sulphur (yellow), hydrogen (white), nitrogen (blue), chloride (green) and bromide (garnet). See Table 7 for a more detailed description on intermolecular interactions.

IL41–SO_2 system (Fig. 7). The SO_2 molecule also interacts (through both hydrogen atoms) with the cation (d_6 and d_7, d_{12} and d_{13} or d_{20} and d_{21} for IL 41, 42 or 44, respectively). Instead the selected IL, the sum of the electronic density for both intermolecular bonds is $\simeq$0.0190 a.u. Thus, cation···SO_2 contribution to the BE is similar for all ILs within set V.

Table 7 Intermolecular distances (d) along the electronic density values (ρ) of [EMIm][Cl] (45), [EMIm][Br] (48) and [EMIM][I] (51). See Fig. 15 for labeling

	IL		IL···SO_2	
	d/Å	ρ/a.u.	d/Å	ρ/a.u.
45 – [EMIm][Cl]				
d_1	1.982	0.0264	2.515	0.0149
d_2	2.750	0.0096	2.681	0.0111
d_3			2.589	0.0474
d_4			2.668	0.0110
d_5			2.367	0.0115
48 – [EMIm][Br]				
d_6	2.798	0.0242	2.581	0.0157
d_7	2.865	0.0101		
d_8	2.861	0.0095	2.754	0.0117
d_9			2.709	0.0455
d_{10}			2.112	0.0189
d_{11}			2.321	0.0125
51 – [EMIm][I]				
d_6	2.987	0.0218	2.753	0.0149
d_7	3.041	0.0088		
d_8	3.075	0.0099	2.963	0.0095
d_9			2.775	0.0455
d_{10}			2.121	0.0182
d_{11}			2.383	0.0134

Set VI is devoted to those ILs based on imidazolium cations and halides (IL 44–55). Keeping constant the halide, $[EMIM]^+$ cation always provides the lowest K_H values, while for the same cation K_H increases from chloride to bromide. Similar trends are noted for $|BE'|$ (see Fig. 7), *i.e.*, high K_H is related with low $|BE'|$. The elected halides in this work gave $|BE|$ values ($\simeq$52.18 kJ mol^{-1}) lower than other anions; even though this $|BE|$ is larger than those obtained for imidazolium cations ($\simeq$35.99 kJ mol^{-1}). For ILs 45–55, cation···SO_2 and anion···SO_2 contributions take values of around 8.00 kJ mol^{-1} and 88 kJ mol^{-1}. Halide effects on the SO_2 adsorption mechanism have been analyzed for ILs based on the $[EMIM]^+$ cation as a function of the anion. Optimized structure for [EMIM][Cl]and [EMIM][Br] (optimized structures for [EMIM][I] is not displayed since similar results to [EMIM][Br] are obtained) are shown in Fig. 15, while the main structural parameter of intermolecular interactions along their electronic density values are collected in Table 7. As expected, the main interaction between both ions is a hydrogen bond between the halide and the H atom located in position 2 (d_1 or d_6 for IL 45 or 48/51, respectively), which is weakened in the presence of SO_2 molecule. For IL···SO_2 systems, S···X (X = Cl, Br or I) is the main interaction (labelled as d_3 or d_9 for IL 45 or 48/51, respectively), while two O···H intermolecular bonds are also found between SO_2 and the cation. As seen in Table 6, electronic density for d_6 is much greater than those of cation···SO_2 interactions in concordance with its larger contribution from $[Cl]^-$···SO_2 interaction. The same behaviour is also noted for ILs 48 and 51.

4. Conclusions

This contribution reports a density functional theory (DFT) on several ILs, for which high SO_2 solubility is expected. This work

is divided into three parts: (i) we selected a set of ILs which should provide high efficiency for SO_2 capture. For this, a screening of a large number of ILs *via* the COSMO-RS method was done; (ii) binding energies between SO_2 and ILs were analyzed intensely through DFT simulations for a set of 55 ILs, which provided high efficiency in SO_2 capture according to the COSMO-RS method; (iii) intermolecular interaction for some representative ILs were deeply studied through the AIM theory aimed at obtaining some information on the SO_2 adsorption mechanism at the molecular level. The results evidenced the ability of the selected cations and anions to interact with the SO_2 molecule, which is stronger for anion$\cdots$$SO_2$ interactions. Thus, anion$\cdots$$SO_2$ interactions are ruled by a strong charge transfer from the anion to SO_2 molecule. For the ILs$\cdots$$SO_2$ system, the total binding energy (BE) has been decomposed in the contributions from the interactions between ions, anion$\cdots$$SO_2$ and cation$\cdots$$SO_2$. The interaction between both ions always provided the largest contribution to the total binding energy. Then, the binding energy related with SO_2 capture by ILs was also calculated considering the ILs as a whole (BE′). A value of around 36.58 kJ mol^{-1} (for CO_2 capture by [EMIM][NTf_2] IL, which was taken as a pivotal reference for comparison purposes) as a low limit; all ILs yield larger binding energies. Most of them provide values of around 45.0 kJ mol^{-1}. Therefore, all of them would provide high SO_2 capture efficiency. Through the comparison between ion$\cdots$$SO_2$ contributions and BE′, we could obtain some information on what ions mainly govern the SO_2 capture within the ILs. In most cases, SO_2 capture would be mainly ruled out by the anion or by both ions. Even if the SO_2 capture mechanism at the molecule level depends on each ILs, some common features as found for related ions. Even though, a statistical analysis of binding energies of IL–SO_2 systems as a function of ion–SO_2 and cation–anion ones brings to light that SO_2 adsorption by ILs at the molecular level is mainly ruled by anion–SO_2 interaction and cation–anion as well. Thus, qualitative trends on SO_2 capture by ILs can be obtained only based on the study of anion–SO_2 and isolated ILs systems. Systematic research on ILs for SO_2 capture allow increase of our knowledge about those factors which could be controlled at the molecular level, allowing an approach up to the rational design of task-specific ILs for future applied studies.

Acknowledgements

Gregorio García acknowledges the funding by Junta de Castilla y León (Spain), cofunded by European Social Fund, for a postdoctoral contract. Santiago Aparicio acknowledges the funding by Ministerio de Economía y Competitividad (Spain, project CTQ2013-40476-R) and Junta de Castilla y León (Spain, project BU324U14). Mert Atilhan acknowledges support of an NPRP grant (No: 6-330-2-140) from the Qatar National Research Fund. The statements made herein are solely the responsibility of the authors.

References

1 S. J. Smith, J. van Aardenne, Z. Klimont, R. J. Andres, A. Volke and S. Delgado Arias, *Atmos. Chem. Phys.*, 2011, **11**, 1101–1116.
2 G. Cui, C. Wang, J. Zheng, Y. Guo, X. Luo and H. Li, *Chem. Commun.*, 2012, **48**, 2633–2635.
3 J. Huang, A. Riisager, P. Wasserscheid and R. Fehrmann, *Chem. Commun.*, 2006, 4027–4029.
4 Z. Z. Yang, L. N. He, Y. N. Zhao and B. Yu, *Environ. Sci. Technol.*, 2013, **47**, 1598–1605.
5 D. Yang, M. Hou, H. Ning, J. Ma, X. Kang, J. Zhang and B. Han, Reversible Capture of SO_2 through Functionalized Ionic Liquids, *ChemSusChem*, 2013, **6**(7), 1191–1195.
6 S. Tian, Y. Hou, W. Wu, S. Ren and C. Zhang, *RSC Adv.*, 2013, **3**, 3572–3577; X. L. Yuan, S. J. Zhang and X. M. Lu, *J. Chem. Eng. Data*, 2007, **52**, 596–599; S. Ren, Y. Hou, W. Wu, Q. Liu, Y. Xiao and X. Chen, *J. Phys. Chem. B*, 2010, **114**, 2175–2179; G. Cui, J. Zheng, X. Luo, W. Lin, F. Ding, H. Li and C. Wang, *Angew. Chem., Int. Ed.*, 2013, **52**, 10620–10624.
7 G. Yu and X. Chen, *J. Phys. Chem. B*, 2011, **115**, 3466–3477.
8 S. Ren, Y. Hou, S. Tian, X. Chen and W. Wu, *J. Phys. Chem. B*, 2013, **117**, 482–2486.
9 Z. Lei, C. Dai and B. Chen, *Chem. Rev.*, 2013, **114**, 1289–1326.
10 S. Aparicio and M. Atilhan, *Energy Fuels*, 2010, **24**, 4989–5001; S. Aparicio and M. Atilhan, *J. Phys. Chem. B*, 2012, **116**, 9171–9185; F. Karadas, M. Atilhan and S. Aparicio, *Energy Fuels*, 2010, **24**, 5817–5828; D. H. Zaitsau, A. V. Yermalayeu, S. P. Verevkin, J. E. Bara and A. D. Stanton, *Ind. Eng. Chem. Res.*, 2013, **52**, 16615–16621; C. Wang, X. Luo, H. Luo, D. E. Jiang, H. Li and S. Dai, *Angew. Chem., Int. Ed.*, 2011, **50**, 4918–4922; X. Zhang, H. Dong, Z. Zhao, S. Zhang and Y. Huang, Carbon capture with ionic liquids: overview and progress, *Energy Environ. Sci.*, 2012, **5**, 6668–6681.
11 F. Karadas, B. Köz, J. Jacquemin, E. Deniz, D. Rooney, J. Thompson, C. T. Yavuz, M. Khraisheh, S. Aparicio and M. Atilhan, *Fluid Phase Equilib.*, 2013, **351**, 74–86.
12 V. Sanz, R. Alcalde, M. Atilhan and S. Aparicio, *J. Mol. Model.*, 2014, **20**, 1–14.
13 S. Aparicio, M. Atilhan, M. Khraisheh, R. Alcalde and J. Fernández, *J. Phys. Chem. B*, 2011, **115**, 12487–12498.
14 J. Palomar, M. González-Miquel, A. Polo and F. Rodríguez, *Ind. Eng. Chem. Res.*, 2011, **50**, 3452–3463.
15 J. Earle-Martyn and R. Seddon-Kenneth, Green Solvents for the Future, in *Clean Solvents*, American Chemical Society, 2002; J. S. Wilkes, *Green Chem.*, 2002, **4**, 73–80; R. D. Rogers and K. R. Seddon, *Science*, 2003, 792–793.
16 O. Hollóczki, Z. Kelemen, L. Könczöl, D. Szieberth, L. Nyulászi, A. Stark and B. Kirchner, *ChemPhysChem*, 2013, **14**, 315–320; K. M. Gupta and J. Jiang, *J. Phys. Chem. C*, 2014, **118**, 3110–3118; P. Gu, R. Lü, S. Wang, Y. Lu and D. Liu, *Comput. Theor. Chem.*, 2013, **1020**, 22–31; F. Yan, M. Lartey, K. Damodaran, E. Albenze, R. L. Thompson, J. Kim, M. Haranczyk, H. B. Nulwala, D. R. Luebke and B. Smit, *Phys. Chem. Chem. Phys.*, 2013, **15**, 3264–3272;

C. Wu, T. P. Senftle and W. F. Schneider, *Phys. Chem. Chem. Phys.*, 2012, **14**, 13163–13170; B. Gurkan, B. F. Goodrich, E. M. Mindrup, L. E. Ficke, M. Massel, S. Seo, T. P. Senftle, H. Wu, M. F. Glaser, J. K. Shah, E. J. Maginn, J. F. Brennecke and W. F. Schneider, *J. Phys. Chem. Lett.*, 2010, **1**, 3494–3499.

17 G. B. Damas, A. B. A. Dias and L. T. Costa, *J. Phys. Chem. B*, 2014, **118**, 9046–9064.

18 A. Klamt, *COSMO-RS: From Quantum Chemistry to Fluid Phase Thermodynamcis and Drug Design*, Elsevier, Amsterdam, 2005; F. Eckert and A. Klamt, *AIChE J.*, 2002, **48**, 369–385.

19 M. J. Frisch, G. W. Trucks, H. B. Schlegel, G. E. Scuseria, M. A. Robb, J. R. Cheeseman, G. Scalmani, V. Barone, B. Mennucci, G. A. Petersson, H. Nakatsuji, M. Caricato, X. Li, H. P. Hratchian, A. F. Izmaylov, J. Bloino, G. Zheng, J. L. Sonnenberg, M. Hada, M. Ehara, K. Toyota, R. Fukuda, J. Hasegawa, M. Ishida, T. Nakajima, Y. Honda, O. Kitao, H. Nakai, T. Vreven, J. A. Montgomery, Jr., J. E. Peralta, F. Ogliaro, M. Bearpark, J. J. Heyd, E. Brothers, K. N. Kudin, V. N. Staroverov, R. Kobayashi, J. Normand, K. Raghavachari, A. Rendell, J. C. Burant, S. S. Iyengar, J. Tomasi, M. Cossi, N. Rega, J. M. Millam, M. Klene, J. E. Knox, J. B. Cross, V. Bakken, C. Adamo, J. Jaramillo, R. Gomperts, R. E. Stratmann, O. Yazyev, A. J. Austin, R. Cammi, C. Pomelli, J. W. Ochterski, R. L. Martin, K. Morokuma, V. G. Zakrzewski, G. A. Voth, P. Salvador, J. J. Dannenberg, S. Dapprich, A. D. Daniels, ö. Farkas, J. B. Foresman, J. V. Ortiz, J. Cioslowski and D. J. Fox, *Gaussian 09, Revision D.01*, Gaussian, Inc., Wallingford, CT, USA, 2009.

20 C. Lee, W. Yang and R. G. Parr, *Phys. Rev. B: Condens. Matter Mater. Phys.*, 1988, **37**, 785–789; A. D. Becke, *J. Chem. Phys.*, 1993, **98**, 5648; A. D. Becke, *Phys. Rev. A: At., Mol., Opt. Phys.*, 1988, **38**, 3098–3100.

21 A. J. Cohen, P. Mori-Sánchez and W. Yang, *Chem. Rev.*, 2012, **112**, 289–320.

22 S. Grimme, *J. Comput. Chem.*, 2006, **27**, 1787–1799.

23 T. Schwabe and S. Grimme, *Phys. Chem. Chem. Phys.*, 2007, **9**, 3397–3406; S. Zahn and B. Kirchner, *J. Phys. Chem. A*, 2008, **112**, 8430–8435; S. Grimme, W. Hujo and B. Kirchner, *Phys. Chem. Chem. Phys.*, 2012, **14**, 4875–4883; E. I. Izgorodina, U. L. Bernard and D. R. MacFarlane, *J. Phys. Chem. A*, 2009, **113**, 7064–7072; S. Zahn, F. Uhlig, J. Thar, C. Spickermann and B. Kirchner, *Angew. Chem., Int. Ed.*, 2008, **47**, 3639–3641.

24 J. Marten, W. Seichter, E. Weber and U. Bohme, *CrystEngComm*, 2008, **10**, 541–547.

25 S. Simon, M. Duran and J. J. Dannenberg, *J. Chem. Phys.*, 1996, **105**, 11024; S. F. Boys and F. Bernardi, *Mol. Phys.*, 1970, **19**, 553–566.

26 R. A. Ando, L. J. A. Siqueira, F. C. Bazito, R. M. Torresi and P. S. Santos, *J. Phys. Chem. B*, 2007, **111**, 8717–8719; L. J. A. Siqueira, R. A. Ando, F. C. C. Bazito, R. M. Torresi, P. S. Santos and M. C. C. Ribeiro, *J. Phys. Chem. B*, 2008, **112**, 6430–6435.

27 R. S. Mulliken, *J. Chem. Phys.*, 1955, **23**, 1833.

28 J. J. Philips, M. A. Hudspeth, Jr, P. M. Browne and J. E. Peralta, *Chem. Phys. Lett.*, 2010, **495**, 146–150.

29 C. M. Breneman and K. B. Wiberg, *J. Comput. Chem.*, 1990, **11**, 361–373.

30 I. Bandrés, R. Alcalde, C. Lafuente, M. Atilhan and S. Aparicio, *J. Phys. Chem. B*, 2011, **115**, 12499–12513.

31 R. F. W. Bader, *Atoms in Molecules: a Quantum Theory*, Oxford, 1990.

32 T. Lu and F. Chen, *J. Comput. Chem.*, 2012, **33**, 580–592.

33 J. Palomar, V. R. Ferro, J. S. Torrecilla and F. Rodríguez, *Ind. Eng. Chem. Res.*, 2007, **46**, 6041–6048; J. Palomar, J. S. Torrecilla, V. R. Ferro and F. Rodríguez, *Ind. Eng. Chem. Res.*, 2009, **48**, 2257–2265; A. Klamt, *Wiley Interdiscip. Rev.: Comput. Mol. Sci.*, 2011, **1**, 699–709; M. A. Diedenhofen and A. Klamt, *Fluid Phase Equilib.*, 2010, **294**, 31–38; X. Zhang, Z. Liu and W. Wang, *AIChE J.*, 2008, **54**, 2717–2728; M. B. Miller, D. L. Chen, H. B. Xie, D. R. Luebke, J. Karl Johnson and R. M. Enick, *Fluid Phase Equilib.*, 2009, **287**, 26–32; R. Franke, B. Hannebauer and S. A. Jung, *Chem. Eng. Technol.*, 2010, **33**, 251–257; N. A. Manan, C. Hardacre, J. Jacquemin, D. W. Rooney and T. G. Youngs, *J. Chem. Eng. Data*, 2009, **54**, 2005–2022.

34 M. González-Miquel, J. Palomar and S. Omar, *Ind. Eng. Chem. Res.*, 2011, **50**, 5739–5748.

35 M. González-Miquel, J. Bedia, J. Palomar and F. Rodríguez, *J. Chem. Eng. Data*, 2014, **59**, 212–217.

36 M. Atilhan, J. Jacquemin, D. Rooney, M. Khraisheh and S. Aparicio, *Ind. Eng. Chem. Res.*, 2013, **52**, 16774–16785.

37 G. García, M. Atilhan and S. Aparicio, *Chem. Phys. Lett.*, 2014, **610**, 267–272.

